Compensation Effect for the Kinetics of Adsorption/Desorption of Gases/Vapors on Microporous Carbon Materials

ARTICLE *in* LANGMUIR · JULY 2000

Impact Factor: 4.46 · DOI: 10.1021/la9916528

2 AUTHORS:

Ashleigh Fletcher
University of Strathclyde
43 PUBLICATIONS **2,921** CITATIONS
SEE PROFILE

Keith Mark Thomas
Newcastle University
198 PUBLICATIONS **10,365** CITATIONS
SEE PROFILE

Compensation Effect for the Kinetics of Adsorption/Desorption of Gases/Vapors on Microporous Carbon Materials

Ashleigh J. Fletcher and K. Mark Thomas*

Northern Carbon Research Laboratories, Department of Chemistry, Bedson Building, University of Newcastle-upon-Tyne, Newcastle-upon-Tyne, NE1 7RU, UK

Received December 17, 1999. In Final Form: March 31, 2000

Preliminary studies of adsorption kinetics on activated carbon provided some tentative evidence for a possible compensation effect where the activation energies and ln(preexponential factors) obtained from the Arrhenius equation obey a linear correlation. However, a detailed analysis was not carried out. The adsorption characteristics of a series of *n*-alcohol vapors on the activated carbon BAX950 were investigated over the relative pressure range $p/p^o = 0-0.97$, for temperatures in the range 288−318 K. These data, in combination with our previous results for water, *n*-octane, and *n*-nonane adsorption provide a comprehensive adsorption kinetic study on an active carbon covering a full range of adsorptives with varying hydrophilic/hydrophobic character to establish the general validity, applicability, and mechanism of the compensation effect. The results are discussed with reference to the pore structure and the adsorption mechanism. Detailed comparisons show that the compensation effect is a general phenomenon for adsorption and desorption on microporous carbons and may extend further to other porous systems.

1. Introduction

Activated carbon filters have many practical applications in the removal of toxic volatile organic compounds (VOCs) from air streams.[1,2] Adsorption on active carbons is very complex because of the variety of sites available for adsorption and the heterogeneous nature of the porous structure. Activated carbons have hydrophobic sites consisting of the graphene basal plane layers and hydrophilic sites comprising the functional groups. The hydrophobic graphene layer surfaces act as primary adsorption sites for hydrocarbons, whereas the hydrophilic oxygen functional groups are primary sites for adsorption of water vapor. The adsorption isotherm is a function of the concentration and distribution of the adsorption sites and pore structure of the adsorbent and the adsorptive structure and vapor pressure.

Both the adsorption kinetics and thermodynamics are of critical importance in assessing the performance of active carbon beds for the adsorption of pollutant species. However, the available information on the adsorption kinetics of gases and vapors is limited and mainly confined to studies of adsorption on carbon molecular sieves (CMS). Studies of the adsorption of gases such as oxygen, nitrogen, and carbon dioxide on a carbon molecular sieve (CMS) have shown that the adsorption kinetics follow a linear driving force (LDF), a combined barrier resistance/diffusion model, or Fickian diffusion depending on the experimental conditions, the adsorptive, and the structure of the adsorbent.[3,4] The adsorption of water vapor on a CMS, a highly microporous coconut shell (C1), and a wood-derived active carbon (BAX950) also follow an LDF[5−7] model. *n*-Octane adsorption on active carbon BAX950 also obeys an LDF model for a large portion of the uptake isotherm while above a relative pressure of 0.175 the kinetics follow a combined barrier resistance/diffusion model.[8] However, the dependence of rate constant on the amount adsorbed is a function of the adsorption mechanism.

Previous studies of the activation energies for the adsorption kinetics of water, *n*-octane, and *n*-nonane vapors on active carbons have provided some tentative evidence for a possible compensation effect where the activation energies and ln(preexponential factors) have a linear correlation.[5,8] These observations are surprising because the adsorption mechanisms for water and hydrocarbon vapors on active carbons are very different. The adsorption of water vapor initially occurs on the hydrophilic functional groups followed by the development of clusters of water molecules around these functional groups leading to eventual bridging between clusters and pore filling.[9] In contrast, hydrocarbon adsorption takes place on the graphene layers. Therefore, since these two situations represent the two extremes in terms of adsorption mechanism, it is possible that the compensation effect is a general effect in adsorption kinetics.

The objective of this investigation was to study a range of adsorptives with varying hydrophilic/hydrophobic character to establish if the compensation effect was observed for a full range of adsorption characteristics. The study involves an investigation of the adsorption kinetics of a series of *n*-alcohols of varying chain length so as to vary the hydrophilic/hydrophobic character of the adsorptive to produce detailed kinetic data for a suite of adsorptive vapors from water to hydrocarbons on a single adsorbent. This study is part of a research program to investigate the effect of changes in atmospheric conditions for vapor adsorption at very low pressures to understand the

* Author to whom all correspondence should be addressed. E-mail: mark.thomas@ncl.ac.uk.

(1) Hassler, W. *Activated Carbon*; John Wiley: New York, 1954.
(2) *Volatile Organic Compounds in the Atmosphere*; Hester, R. E., Harrison, R. M., Eds.; The RSC: Cambridge, 1995.
(3) Reid, C. R.; O'koye, I. P.; Thomas, K. M. *Langmuir* **1998**, *14*, 2415.
(4) Reid, C. R.; Thomas, K. M. *Langmuir* **1999**, *15*, 3206.
(5) Harding, A. W.; Foley, N. J.; Norman, P. R.; Francis, D. C.; Thomas, K. M. *Langmuir* **1998**, *14*, 3858.
(6) O'Koye, I. P.; Benham, M.; Thomas, K. M. *Langmuir* **1997**, *13*, 4054.
(7) Foley, N. J.; Forshaw, P. L.; Thomas, K. M.; Stanton, D.; Norman, P. R. *Langmuir* **1997**, *13*, 2083.
(8) Fletcher, A. J.; Thomas, K. M. *Langmuir* **1999**, *15*, 6908.
(9) Muller, E. A.; Rull, L. F.; Vega, L. F.; Gubbins, K. E. *J. Phys. Chem.* **1996**, *100*, 1189.

10.1021/la9916528 CCC: $19.00
Published on Web 06/23/2000

performance of activated carbons in filtering processes, in terms of pore structure and the adsorption mechanism.

2. Experimental Section

2.1. Materials Used. Carbon BAX950, a wood-based activated carbon, was obtained from the Westvaco Corp. The particle size fraction of this carbon is 1−2 mm. The adsorbates used were methanol (99.8% purity), supplied by B. D. H. Ltd., Poole, England; and ethanol (99.5%), propan-1-ol (99.7%), and butan-1-ol (99.8%), supplied by Aldrich Chemical Co., Milwaukee, WI.

2.2. Adsorption Studies. The apparatus used was an intelligent gravimetric analyzer (IGA) supplied by Hiden Analytical Ltd.: Warrington, UK. This apparatus is an ultrahigh vacuum system which allows isotherms and the corresponding kinetics of adsorption and desorption to be determined, for set pressure steps.[10] The balance and pressure control system were fully thermostated to ±0.2 K to eliminate changes in the external environment. The microbalance had a long-term stability of ±1 μg with a weighing resolution of 0.2 μg. The carbon sample (100 ± 1 mg) was outgassed to a constant weight, at a pressure of $<10^{-6}$ Pa at 473 K. The liquid used to generate the vapor was degassed fully by repeated evacuation and vapor equilibration cycles of the liquid supply side of the vapor reservoir. The vapor pressure was gradually increased, over a time scale of ∼30 s to prevent disruption of the microbalance, until the desired value was achieved. Pressure control was via the use of two transducers with ranges 0−0.2 and 0−10 kPa, each with an accuracy of 0.02% of the specified range. The pressure was maintained at the set point by active computer control of the inlet/outlet valves throughout the duration of the experiment. Pressure steps in the range of p/p^o values 0−0.97 were used to obtain the isotherm. The mass uptake was measured as a function of time and the approach to equilibrium monitored in real time with a computer algorithm. After equilibrium was established, the vapor pressure was increased to the next set pressure value and the subsequent uptake was measured until equilibrium was reestablished. The increase in weight due to adsorption for each pressure step was used to calculate the kinetic parameters for adsorption using an appropriate kinetic model. The errors in the calculated rate constants were typically better than ±2%. The sample temperature was monitored throughout the experiment and the variation in sample temperature was minimal (<0.1 K). In the case of desorption, the reverse procedure was carried out. The adsorption isotherms for various temperatures were carried out in steps of relative pressure thereby corresponding to steps of surface coverage. The saturated vapor pressures were calculated using the following equation:[11]

$$\log p = A - \frac{B}{T + C} \qquad (1)$$

where p is the saturated vapor pressure (Torr), T is the temperature in degrees Celsius and A, B, and C are constants defined by the adsorbate: methanol, $A = 7.89750$, $B = 1474.08$, $C = 229.13$; ethanol, $A = 8.32109$, $B = 1718.10$, $C = 237.52$; propan-1-ol, $A = 7.84767$, $B = 1499.21$, $C = 204.64$; butan-1-ol, $A = 7.47680$, $B = 1362.39$, $C = 178.77$.

3. Results

3.1. Adsorption Isotherm Measurements. The adsorption isotherms for water, methanol, ethanol, propan-1-ol, and butan-1-ol on BAX950 are shown in Figure 1 together with the isotherms previously obtained for *n*-octane and *n*-nonane. Comparison of the set of adsorption isotherms shows that they change progressively from type I to type III in the IUPAC classification scheme. The water adsorption isotherm is in excellent agreement with previous studies,[5] but a higher resolution was used in this study for detailed comparison with other adsorptives at low relative pressure (p/p^o). The adsorption isotherms

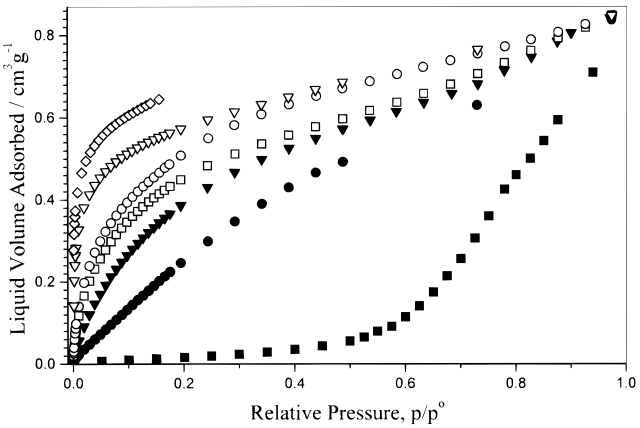

Figure 1. Adsorption isotherms for water (■), methanol (●), ethanol (▼), propan-1-ol (□), butan-1-ol (○), *n*-octane (▽), and *n*-nonane (◇) at 303 K on active carbon BAX950.

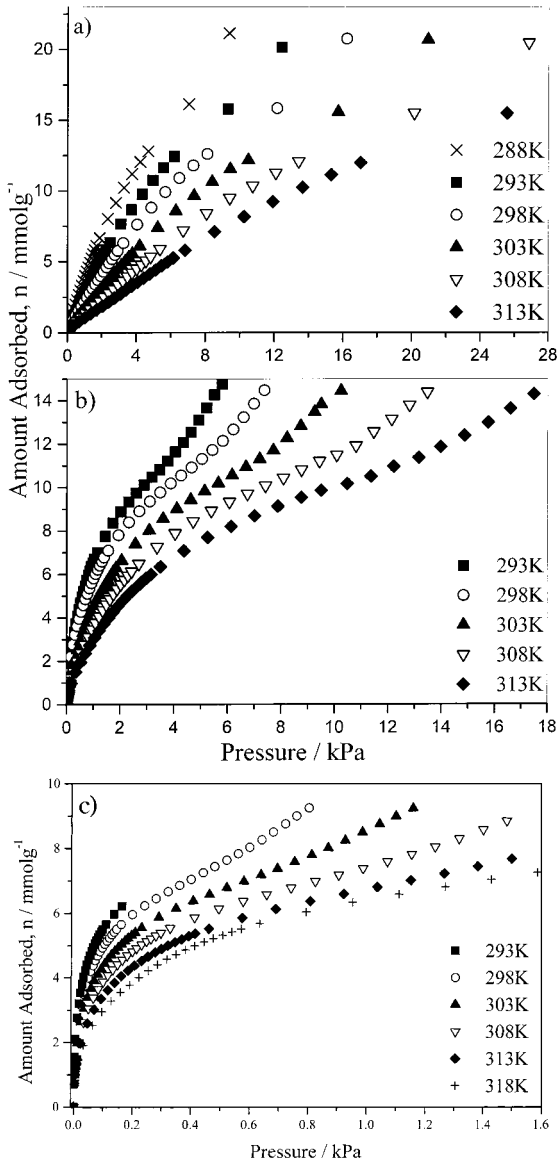

Figure 2. Adsorption isotherms for (a) methanol, (b) ethanol, and (c) butan-1-ol adsorption on active carbon BAX950.

of methanol, ethanol, propan-1-ol, and butan-1-ol on BAX950 are all classified as type II isotherms in the IUPAC classification scheme, as observed previously for adsorption on active carbons[12−17] and zeolites.[18,19] The sets of

(10) Benham, M. J.; Ross, D. K. *Z. Phys. Chem.* **1989**, *163*, 25.
(11) *Lange's Handbook of Chemistry*, 15th ed.; McGraw-Hill: New York, 1999.

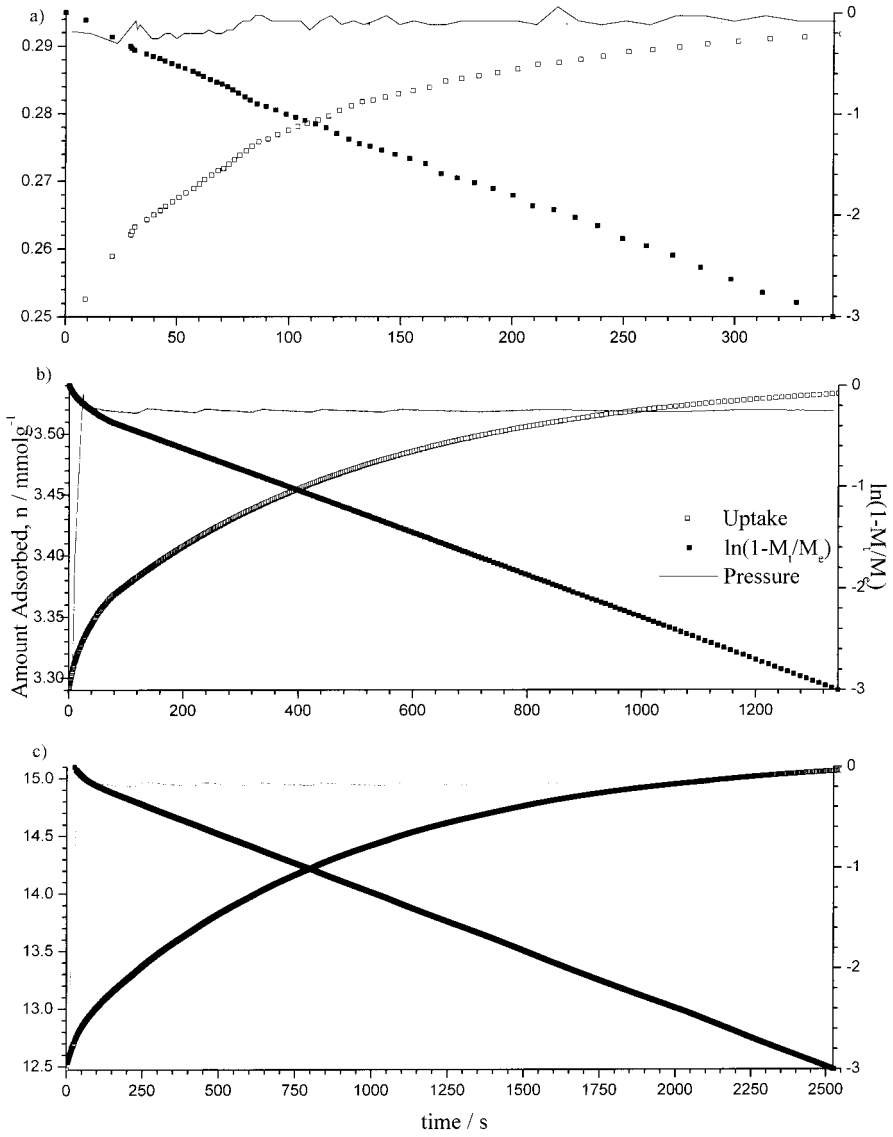

Figure 3. Kinetic profiles for methanol adsorption on active carbon BAX950 at (a) 288 K, $p/p^o = 0.00194-0.00292$ (32.2−48.6 Pa); (b) 288 K, $p/p^o = 0.0972-0.1068$ (1.618−1.785 kPa); (c) 288 K, $p/p^o = 0.4868-0.7296$ (8.11−12.15 kPa).

isotherms obtained for methanol, ethanol, and butan-1-ol adsorption at various temperatures shown in Figure 2 gave very good agreement on a relative pressure basis. The total adsorption uptake decreased with increasing temperature when plotted against total pressure, as expected for physisorption.

Desorption of preadsorbed methanol and ethanol vapors from BAX950 was also investigated, over the same temperature and pressure ranges, and no significant hysteresis was observed below $p/p^o = 0.5$, at 298 K.

3.2. Adsorption Kinetics. The kinetics of adsorption of methanol, ethanol, propan-1-ol, and butan-1-ol on BAX950 follow a linear driving force (LDF) mass-transfer model[3−8,20] up to $p/p^o \sim 0.97$. The LDF model is described by the equation

$$\frac{M_t}{M_e} = 1 - e^{-kt} \qquad (2)$$

where M_t is the uptake at time t, M_e is the equilibrium uptake, and k is the rate constant. A plot of $\ln(1 - M_t/M_e)$ versus time is linear with a gradient equal to the rate constant.

Figure 3 shows plots of $\ln(1 - M_t/M_e)$ versus time for three typical adsorption steps for methanol. Each graph shows that the adsorption kinetics obeys the LDF model and represents pressure increments in a different pressure region to prove that the model holds regardless of the position on the isotherm in the range $p/p^o \sim 0-0.97$. The adsorption uptakes obey the LDF model for >90% of the total uptake for a particular pressure step, and the kinetic data are given in Table 1. The slight curve in the initial uptake region is due to initial rapid change in the internal vapor pressure of adsorptive in the instrument.

(12) Bradley, R. H.; Rand, B. *J. Colloid Interface Sci.* **1995**, *169*, 168.
(13) Bradley, R. H.; Rand, B. *Carbon* **1991**, *29*, 1165.
(14) da Silva, A. M. G.; Soares, V. A. M.; Calado, J. C.; Brotas de Carvalho, M. *J. Chem. Soc.: Farad.* Trans. **1991**, *87*, 3799.
(15) Rozwadowski, M.; Wojsz, R.; Garbacz, J. K. *Pol. J. Chem.* **1980**, *54*, 1591.
(16) Ohkubo, T.; Iiyama, T.; Nishikawa, K.; Suzuki, T.; Kaneko, K. *J. Phys. Chem. B* **1999**, *103*, 1859.
(17) Rodriguez-Reinoso, F.; Molina-Sabio, M.; Munecas, M. A. *J. Phys. Chem.* **1992**, *96*, 2707.
(18) Izmailova, S. G.; Vasiljeva, E. A.; Karetina, I. V.; Feoktistova, N. N.; Khvoshchev, S. S. *J. Colloid Interface Sci.* **1996**, *179*, 374.
(19) Hunger, B.; Matysik, S.; Heuchel, M.; Einicke, W. D. *Langmuir* **1997**, *13*, 6249.
(20) Braymer, T. A.; Coe, C. G.; Farris, T. S.; Gaffney, T. R.; Schork, J. M.; Armor, J. N. *Carbon* **1994**, *32*, 445.

Table 1. Rate Constants for Adsorption of (a) Methanol and (b) Ethanol on Active Carbon BAX950 Obtained from the LDF Model

	(a) rate constant /(s^{-1}) × 10^{-3} for methanol adsorption						(b) rate constants/((s^{-1}) × 10^{-3} for ethanol adsorption				
p/p^o	288 K	293 K	298 K	303 K	308 K	313 K	293 K	298 K	303 K	308 K	313 K
0−0.0010	2.55 ± 0.03	2.66 ± 0.11	3.91 ± 0.04	4.00 ± 0.06	7.44 ± 0.12	8.67 ± 0.15	2.20 ± 0.02	1.80 ± 0.01	3.40 ± 0.04	3.33 ± 0.03	4.64 ± 0.06
0.0010−0.0019	4.67 ± 0.09	6.08 ± 0.12	7.24 ± 0.14	8.90 ± 0.18	10.02 ± 0.22	12.52 ± 0.16	2.73 ± 0.04	2.47 ± 0.02	4.03 ± 0.05	6.25 ± 0.09	6.86 ± 0.09
0.0019−0.0029	5.68 ± 0.11	6.68 ± 0.12	8.22 ± 0.14	10.01 ± 0.24	10.83 ± 0.27	15.34 ± 0.40	3.24 ± 0.05	3.17 ± 0.04	5.32 ± 0.08	6.18 ± 0.10	7.23 ± 0.12
0.0029−0.0039	5.92 ± 0.13	7.30 ± 0.38	9.12 ± 0.20	10.46 ± 0.27	10.86 ± 0.27	15.92 ± 0.51	3.54 ± 0.05	3.89 ± 0.06	5.55 ± 0.09	6.61 ± 0.12	7.70 ± 0.14
0.0039−0.0049	6.15 ± 0.14	7.50 ± 0.38	9.47 ± 0.21	11.95 ± 0.31	11.79 ± 0.33	15.55 ± 0.56	3.56 ± 0.06	3.83 ± 0.06	5.61 ± 0.10	6.81 ± 0.13	7.76 ± 0.15
0.0049−0.0098	6.79 ± 0.05	8.92 ± 0.08	10.16 ± 0.07	13.76 ± 0.32	15.29 ± 0.30	16.78 ± 0.37	3.75 ± 0.04	4.04 ± 0.06	5.34 ± 0.06	6.66 ± 0.08	7.65 ± 0.10
0.0098−0.0194	8.25 ± 0.10	9.50 ± 0.12	10.13 ± 0.13	12.59 ± 0.27	15.75 ± 0.25	18.05 ± 0.29	3.00 ± 0.02	3.74 ± 0.04	4.28 ± 0.04	5.36 ± 0.06	5.76 ± 0.07
0.0194−0.0292	4.96 ± 0.07	6.55 ± 0.10	8.46 ± 0.14	9.63 ± 0.24	10.99 ± 0.23	12.00 ± 0.26	2.70 ± 0.02	3.23 ± 0.03	3.66 ± 0.04	4.46 ± 0.05	5.32 ± 0.07
0.0292−0.0389	4.24 ± 0.07	5.65 ± 0.10	6.99 ± 0.13	7.32 ± 0.17	8.76 ± 0.19	8.47 ± 0.19	2.37 ± 0.02	3.06 ± 0.03	3.25 ± 0.03	4.16 ± 0.05	4.73 ± 0.07
0.0389−0.0487	3.51 ± 0.06	4.77 ± 0.08	5.64 ± 0.11	5.53 ± 0.13	7.15 ± 0.15	7.76 ± 0.17	2.27 ± 0.02	3.00 ± 0.03	3.05 ± 0.03	3.68 ± 0.05	4.05 ± 0.05
0.0487−0.0584	3.10 ± 0.05	3.77 ± 0.06	4.65 ± 0.08	4.69 ± 0.10	5.83 ± 0.12	5.94 ± 0.12	2.26 ± 0.02	2.96 ± 0.04	2.76 ± 0.03	3.19 ± 0.04	3.61 ± 0.05
0.0584−0.0681	2.54 ± 0.04	3.12 ± 0.05	3.71 ± 0.07	4.36 ± 0.10	4.54 ± 0.08	4.93 ± 0.09	2.17 ± 0.02	2.94 ± 0.04	2.59 ± 0.03	3.04 ± 0.04	3.62 ± 0.05
0.0681−0.0777	2.19 ± 0.03	2.78 ± 0.04	3.35 ± 0.06	3.45 ± 0.07	4.24 ± 0.09	4.74 ± 0.10	2.19 ± 0.03	2.80 ± 0.04	2.65 ± 0.03	2.84 ± 0.03	3.15 ± 0.04
0.0777−0.0876	1.98 ± 0.03	2.55 ± 0.03	3.02 ± 0.05	3.05 ± 0.06	3.87 ± 0.08	4.04 ± 0.07	2.05 ± 0.02	2.69 ± 0.04	2.60 ± 0.03	2.83 ± 0.04	3.13 ± 0.04
0.0876−0.0972	2.02 ± 0.03	2.28 ± 0.03	2.64 ± 0.04	2.94 ± 0.06	3.14 ± 0.05	3.71 ± 0.07	2.13 ± 0.03	2.48 ± 0.03	2.55 ± 0.03	2.76 ± 0.04	2.83 ± 0.04
0.0972−0.1068	1.85 ± 0.02	2.10 ± 0.03	2.51 ± 0.04	2.64 ± 0.04	2.87 ± 0.04	3.24 ± 0.06	1.88 ± 0.02	2.54 ± 0.04	2.21 ± 0.03	2.69 ± 0.04	2.84 ± 0.04
0.1068−0.1167	1.90 ± 0.02	2.00 ± 0.02	2.28 ± 0.03	2.38 ± 0.04	2.66 ± 0.04	3.03 ± 0.05	1.97 ± 0.02	2.46 ± 0.04	2.46 ± 0.03	2.50 ± 0.04	2.85 ± 0.04
0.1167−0.1264	1.75 ± 0.02	1.89 ± 0.03	2.09 ± 0.03	2.80 ± 0.05	2.56 ± 0.04	2.72 ± 0.04	1.75 ± 0.02	2.32 ± 0.03	2.31 ± 0.03	2.45 ± 0.04	2.78 ± 0.04
0.1264−0.1362	1.59 ± 0.02	1.72 ± 0.02	1.93 ± 0.02	2.41 ± 0.04	2.29 ± 0.03	2.68 ± 0.04	1.88 ± 0.02	2.33 ± 0.03	2.36 ± 0.03	2.46 ± 0.04	2.73 ± 0.03
0.1362−0.1458	1.45 ± 0.01	1.66 ± 0.01	1.85 ± 0.02	2.10 ± 0.03	2.33 ± 0.03	2.25 ± 0.03	1.87 ± 0.02	2.37 ± 0.04	2.33 ± 0.03	2.54 ± 0.04	2.79 ± 0.04
0.1458−0.1556	1.44 ± 0.01	1.56 ± 0.02	1.80 ± 0.02	1.88 ± 0.02	2.21 ± 0.03	2.50 ± 0.04	1.87 ± 0.02	2.00 ± 0.02	2.37 ± 0.04	2.36 ± 0.04	2.71 ± 0.05
0.1556−0.1655	1.47 ± 0.01	1.56 ± 0.02	1.67 ± 0.02	1.99 ± 0.03	2.10 ± 0.03	2.17 ± 0.03	2.03 ± 0.04	2.26 ± 0.04	2.37 ± 0.04	2.37 ± 0.03	2.85 ± 0.05
0.1655−0.1752	1.47 ± 0.02	1.53 ± 0.02	1.58 ± 0.02	1.95 ± 0.02	1.99 ± 0.03	2.14 ± 0.03	2.11 ± 0.04	2.23 ± 0.03	2.14 ± 0.03	2.43 ± 0.04	2.61 ± 0.04
0.1752−0.1946	1.40 ± 0.01	1.45 ± 0.01	1.56 ± 0.01	1.70 ± 0.01	1.83 ± 0.02	2.04 ± 0.02	1.72 ± 0.02	1.80 ± 0.03	2.17 ± 0.02	2.27 ± 0.03	2.63 ± 0.03
0.1946−0.2434	1.17 ± 0.01	1.32 ± 0.01	1.39 ± 0.01	1.53 ± 0.01	1.63 ± 0.01	1.74 ± 0.01	1.75 ± 0.02	2.27 ± 0.03	2.08 ± 0.02	2.20 ± 0.02	2.50 ± 0.03
0.2434−0.2919	1.19 ± 0.01	1.28 ± 0.01	1.32 ± 0.01	1.37 ± 0.01	1.50 ± 0.01	1.70 ± 0.01	1.95 ± 0.02	2.12 ± 0.02	2.11 ± 0.02	2.23 ± 0.02	2.55 ± 0.02
0.2919−0.3407	1.14 ± 0.01	1.23 ± 0.01	1.28 ± 0.01	1.40 ± 0.01	1.47 ± 0.01	1.61 ± 0.01	1.96 ± 0.02	2.24 ± 0.02	2.23 ± 0.02	2.16 ± 0.02	2.63 ± 0.02
0.2407−0.3891	1.11 ± 0.01	1.00 ± 0.01	1.27 ± 0.01	1.34 ± 0.01	1.39 ± 0.01	1.53 ± 0.01	1.98 ± 0.02	2.11 ± 0.02	2.35 ± 0.02	2.29 ± 0.02	2.46 ± 0.02
0.3891−0.4380	1.11 ± 0.01	1.19 ± 0.01	1.26 ± 0.01	1.34 ± 0.01	1.43 ± 0.01	1.57 ± 0.01	1.98 ± 0.02	2.13 ± 0.02	2.28 ± 0.02	2.45 ± 0.03	2.26 ± 0.02
0.4380−0.4868	1.21 ± 0.01	1.19 ± 0.01	1.26 ± 0.01	1.45 ± 0.01	1.51 ± 0.01	1.54 ± 0.01	1.92 ± 0.02	1.92 ± 0.02	2.01 ± 0.02	2.33 ± 0.02	2.16 ± 0.02

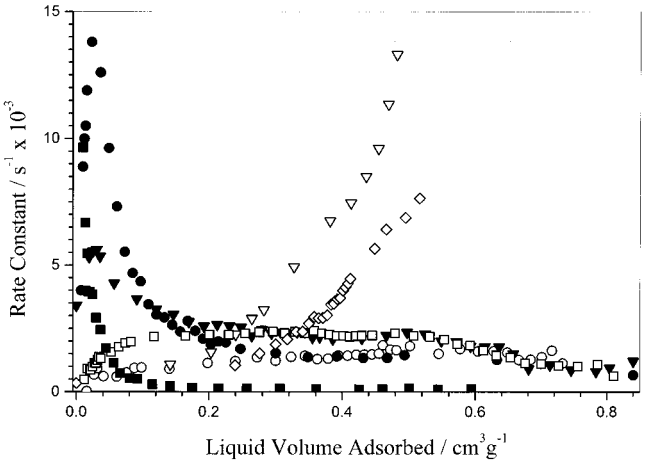

Figure 4. Variation in rate constant for adsorption of water (■), methanol (●), ethanol (▼), propan-1-ol (□), butan-1-ol (○), *n*-octane (▽), and *n*-nonane (◇) with the amount adsorbed on active carbon BAX950 at 303 K.

Table 2. Rate Constants for Adsorption of Propan-1-ol on Activated Carbon BAX950 at 303 K Obtained from the LDF Model

p/p^o	$k/(s^{-1}) \times 10^{-4}$	p/p^o	$k/(s^{-1}) \times 10^{-4}$
0−0.00010	4.92 ± 0.03	0.10709−0.11653	23.11 ± 0.22
0.00010−0.00020	9.13 ± 0.09	0.11653−0.12613	22.58 ± 0.27
0.00020−0.00031	8.59 ± 0.06	0.12613−0.13648	22.11 ± 0.33
0.00031−0.00042	9.86 ± 0.08	0.13648−0.14594	22.21 ± 0.30
0.00042−0.00052	11.39 ± 0.08	0.14594−0.15557	21.82 ± 0.31
0.00052−0.00062	11.33 ± 0.09	0.15557−0.16498	22.02 ± 0.33
0.00062−0.00072	12.50 ± 0.11	0.16498−0.17518	22.25 ± 0.23
0.00072−0.00083	13.78 ± 0.12	0.17518−0.19435	22.29 ± 0.16
0.00083−0.00097	13.15 ± 0.10	0.19435−0.24283	23.08 ± 0.19
0.00097−0.00194	15.69 ± 0.16	0.24283−0.29214	22.12 ± 0.20
0.00194−0.00291	17.82 ± 0.18	0.29214−0.34022	21.82 ± 0.19
0.00291−0.00389	19.27 ± 0.21	0.34022−0.38885	20.75 ± 0.18
0.00389−0.00485	19.76 ± 0.14	0.38885−0.43762	18.93 ± 0.15
0.00485−0.00972	21.79 ± 0.14	0.43762−0.48645	18.30 ± 0.15
0.00972−0.01947	22.08 ± 0.17	0.48645−0.53481	16.36 ± 0.12
0.01947−0.02920	22.56 ± 0.15	0.53481−0.58392	14.48 ± 0.09
0.02920−0.03890	22.50 ± 0.25	0.58392−0.63231	13.64 ± 0.08
0.03890−0.04851	23.10 ± 0.21	0.63231−0.68063	11.38 ± 0.07
0.04851−0.05801	23.52 ± 0.23	0.68063−0.72958	11.00 ± 0.04
0.05801−0.06813	23.77 ± 0.23	0.72958−0.77784	10.40 ± 0.04
0.06813−0.07768	23.24 ± 0.29	0.77784−0.82590	10.10 ± 0.03
0.07768−0.08723	23.70 ± 0.30	0.82590−0.87525	10.78 ± 0.03
0.08723−0.09676	23.10 ± 0.30	0.87525−0.92454	6.33 ± 0.03
0.09676−0.10709	24.19 ± 0.33		

The LDF kinetic model was used to calculate rate constants for the adsorption of methanol, ethanol, propan-1-ol, and butan-1-ol vapor on BAX950 up to $p/p^o \sim 0.97$. Figure 4 shows the variation of adsorption rate constants for the set of alcohols and water vapor on BAX950 at 303 K with surface coverage and comparison with results obtained previously for adsorption of *n*-octane and *n*-nonane.[8] The adsorption rate constants vary with pressure according to the position on the isotherm with the rate constant for adsorption increasing to a maximum at $p/p^o = 0.02$ for methanol and ethanol, then decreasing steadily, with increasing relative pressure and surface coverage. The high-resolution adsorption data for water vapor do not show evidence for a similar peak in the rate constant to those observed for methanol and ethanol. The rate constants for propan-1-ol and butan-1-ol, as given in Tables 2 and 3, increase up to a relative pressure of ∼0.06 and then reach plateaus before decreasing slightly at high p/p^o. It is apparent that the variation in rate constant with surface coverage for the suite of adsorptives studied covers a wide range of behavior. This varies from the rate constant increasing with increasing surface coverage for *n*-octane and *n*-nonane to the rate constant decreasing with increasing surface coverage for water vapor adsorption. There is also intermediate behavior for the adsorption of the set of alcohols.

3.3. Desorption Kinetics of Methanol Vapor. The kinetics of methanol desorption from BAX950 follow an LDF mass-transfer model. The LDF kinetic model can be used to calculate rate constants for the desorption of methanol from BAX950 in the pressure range $p/p^o \sim 0-0.97$. Figure 5 shows the variation of methanol vapor desorption rate constants with surface coverage compared to the rates for methanol adsorption. The rate constants for desorption are similar to those for adsorption, in both magnitude and trend in relation to the isotherm. The rate constants for desorption of water and *n*-octane vapors from active carbon BAX950 also show the same trends relative to the corresponding adsorption rate constants.[5,8] However, the desorption rate constants for *n*-octane are significantly slower than the corresponding adsorption rate constants while the difference is much less marked for water vapor adsorption/desorption.

4. Discussion

4.1. Adsorption Isotherms. The total pore volumes obtained from the isotherms for the set of alcohol vapors studied were calculated from the uptake estimates for $p/p^o = 1$ using the liquid densities. These values are consistent at ∼0.84 $cm^3\ g^{-1}$ and compare favorably with those obtained for *n*-octane adsorption (0.85 $cm^3\ g^{-1}$),[8] *n*-nonane (0.89 $g\ cm^{-3}$),[8] nitrogen (0.83 $cm^3\ g^{-1}$), and water adsorption (0.71 $cm^3\ g^{-1}$).[5] Ohkubo et al. studied the pore-width-dependent ordering of ethanol molecules confined in graphite slit nanospaces in active carbon fibers and KOH-treated active carbon using X-ray diffraction techniques.[16] Analysis of the electron density radial distribution functions and the observation of high densities for adsorbed ethanol indicated that the adsorbate had solidlike ordering at 303 K. However, the total pore volume obtained for adsorption of ethanol on active carbon BAX950 coincides with the nitrogen pore volume and the pore volumes obtained from methanol, propan-1-ol, butan-1-ol, *n*-octane, and *n*-nonane. The results show no evidence for a higher density for ethanol adsorbate on BAX950, although the ordering may have a role in the development of barriers to diffusion at low p/p^o for this porous material. A lower value was obtained for the adsorption of water, which has been noted in previous studies[5−7,13,17,21−25] and is thought to be due to the lower density of the adsorbate due to the inability of adsorbed water to form a full three-dimensional structure in ultramicroporosity. The total pore volumes estimated from the adsorption of various gases and vapors were much greater than the micropore volume obtained from the adsorption of carbon dioxide on BAX950 at 273 K (0.18 $cm^3\ g^{-1}$),[5] suggesting that BAX950 has an extensive meso- and macroporous structure in addition to a microporous structure. The pore size distribution for BAX950 obtained from the nitrogen (77 K) desorption isotherm by the BJH method[26] showed the presence of extensive mesoporosity as well as a significant amount of macroporosity.[8]

(21) Bradley, R. H.; Rand, B. *Carbon* **1993**, *31*, 269.
(22) Arnell, J. C.; McDermott, H. L. *Can. J. Chem.* **1952**, *30*, 177.
(23) Freeman, J. J.; Tomlinson, J. B.; Sing, K. S. W.; Theocharis, C. R. *Carbon* **1993**, *31*, 865.
(24) Freeman, J. J.; Tomlinson, J. B.; Sing, K. S. W.; Theocharis, C. R. *Carbon* **1995**, *33*, 795.
(25) Kaneko, K.; Hanzawa, Y.; Iiyama, T.; Kanda, T.; Suzuki, T. *Adsorption* **1999**, *5*, 7.
(26) Barrett, E. P.; Joyner, L. G.; Halenda, P. P. *J. Am. Chem. Soc.* **1951**, *73*, 373.

Table 3. Rate Constants for Adsorption of Butan-1-ol on Activated Carbon BAX950 Obtained from the LDF Model

	$k/(s^{-1}) \times 10^{-4}$					
p/p^o	293 K	298 K	303 K	308 K	313 K	318 K
0−0.00017	2.87 ± 0.03	3.19 ± 0.02	4.54 ± 0.04	6.09 ± 0.05	6.92 ± 0.09	8.67 ± 0.06
0.00017−0.00032	4.95 ± 0.07	5.29 ± 0.04	8.06 ± 0.07	8.70 ± 0.08	10.96 ± 0.09	14.86 ± 0.13
0.00032−0.00049	5.71 ± 0.05	6.24 ± 0.05	9.05 ± 0.09	11.03 ± 0.10	12.74 ± 0.13	16.75 ± 0.16
0.00049−0.00065	6.20 ± 0.05	7.48 ± 0.05	9.72 ± 0.09	12.13 ± 0.11	14.96 ± 0.15	18.94 ± 0.18
0.00065−0.00099	6.32 ± 0.06	7.95 ± 0.03	10.76 ± 0.11	12.60 ± 0.13	15.96 ± 0.17	19.27 ± 0.20
0.00099−0.00193	7.40 ± 0.06	8.39 ± 0.06	11.56 ± 0.07	14.67 ± 0.09	17.40 ± 0.10	20.37 ± 0.11
0.00193−0.00292	9.24 ± 0.05	9.90 ± 0.04	13.56 ± 0.06	16.38 ± 0.07	19.18 ± 0.08	22.22 ± 0.09
0.00292−0.00386	10.80 ± 0.07	11.69 ± 0.04	15.05 ± 0.09	18.19 ± 0.10	20.80 ± 0.08	23.69 ± 0.08
0.00386−0.00485	11.82 ± 0.06	13.13 ± 0.04	16.46 ± 0.08	19.43 ± 0.09	22.16 ± 0.10	24.89 ± 0.11
0.00485−0.00972	12.40 ± 0.08	13.17 ± 0.05	17.12 ± 0.10	19.74 ± 0.11	23.10 ± 0.13	26.55 ± 0.15
0.00972−0.01945	13.46 ± 0.09	14.59 ± 0.06	17.91 ± 0.11	20.79 ± 0.13	23.54 ± 0.15	
0.01945−0.02918	13.74 ± 0.10	14.70 ± 0.07	18.47 ± 0.14	21.45 ± 0.15	24.90 ± 0.20	
0.02918−0.03892	14.46 ± 0.11	15.01 ± 0.07	19.26 ± 0.15	21.61 ± 0.16	25.58 ± 0.29	
0.03892−0.04865	15.35 ± 0.12	15.72 ± 0.10	19.29 ± 0.16	23.07 ± 0.18	26.56 ± 0.30	
0.04865−0.05834	15.46 ± 0.14	16.31 ± 0.07	20.03 ± 0.18	24.24 ± 0.29	28.23 ± 0.33	
0.05834−0.06808	15.60 ± 0.16	16.68 ± 0.09	20.30 ± 0.20	24.83 ± 0.32	30.22 ± 0.46	
0.06808−0.07781	16.19 ± 0.17	17.10 ± 0.10	20.84 ± 0.20	25.34 ± 0.43	30.33 ± 0.49	
0.07781−0.08755	16.65 ± 0.18	17.30 ± 0.11	21.25 ± 0.21	25.98 ± 0.36	31.16 ± 0.55	
0.08755−0.09728	16.82 ± 0.20	19.09 ± 0.16	21.55 ± 0.28	26.72 ± 0.55	32.03 ± 0.61	
0.09728−0.10701	16.97 ± 0.20	19.88 ± 0.17	22.75 ± 0.28	27.32 ± 0.49	32.55 ± 0.61	
0.10701−0.11674	17.22 ± 0.22	20.89 ± 0.25	24.04 ± 0.47	28.27 ± 0.65	33.51 ± 0.73	
0.11674−0.12648	18.63 ± 0.27	20.05 ± 0.21	26.17 ± 0.51	28.74 ± 0.59		
0.12648−0.13617	19.33 ± 0.28	20.63 ± 0.19	27.09 ± 0.58	29.19 ± 0.64		
0.13617−0.14590	18.08 ± 0.16	20.85 ± 0.25	29.33 ± 0.45	29.68 ± 0.47		
0.14590−0.15575	19.07 ± 0.10	22.49 ± 0.19	23.72 ± 0.18	30.06 ± 0.28		

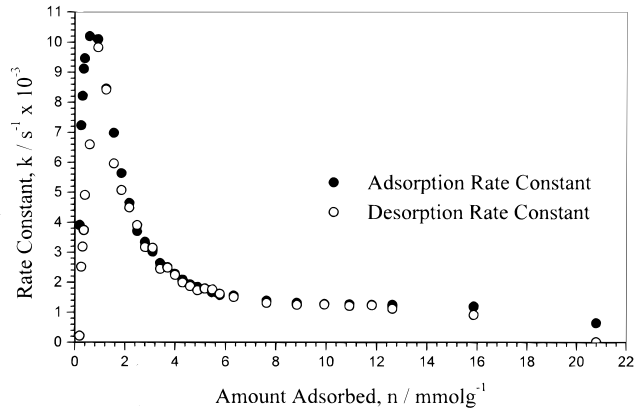

Figure 5. Variation of rate constant with amount adsorbed (n/mmol g^{-1}) for methanol adsorption(●)/desorption (○) from active carbon BAX950 at 303 K.

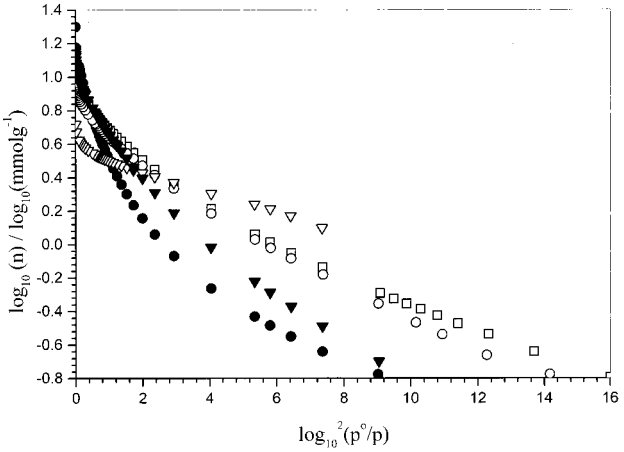

Figure 6. Dubinin−Radushkevich graphs for the adsorption of methanol (●), ethanol (▼), propan-1-ol (□), butan-1-ol (○), and *n*-octane (▽) on active carbon BAX950.

The adsorption isotherms were compared using the Dubinin−Radushkevich (D−R) equation,

$$\log n = \log n_o - B \log^2\left(\frac{p^o}{p}\right) \qquad (3)$$

where n is the amount adsorbed, n_o the amount adsorbed corresponding to the micropore volume, p the pressure, p^o the saturated vapor pressure, and B a constant related to the microporous structure of the adsorbent.[27]

The Dubinin−Radushkevich graphs of the adsorption data for all four alcohols were linear for the low-pressure region of the graph but deviated from linearity at higher pressures, as shown in Figure 6. The changes between the two portions of the plot occur at relative pressures (p/p^o) of ∼0.02 for methanol and ethanol. These values correspond to pore volumes below the micropore volume obtained from carbon dioxide adsorption at 273 K. The D−R graphs for propan-1-ol and butan-1-ol are also shown in Figure 6, together with the corresponding graph for *n*-octane. It is apparent that the deviations for these adsorptives occur at higher relative pressures close to where the rate reaches a plateau. The upward deviation of the D−R plots from linearity indicates filling of available adsorption volume at pressures below that predicted by the micropore distribution function used in the D−R model.[28]

4.2. Thermodynamics of Adsorption. Hysteresis for the ethanol isotherm was insignificant below $p/p^o \sim 0.5$, contrary to previous findings for the adsorption of ethanol on activated carbon.[14] The adsorption isotherm for methanol showed similar hysteresis behavior. The isosteric enthalpies (ΔH_i) and entropies (ΔS_i) of adsorption were calculated at constant surface coverage from the equation

$$\ln(p) = \Delta H_i/RT - \Delta S_i/R \qquad (4)$$

where p is the pressure, R is the gas constant, and T is the temperature.

The isosteric enthaplies of adsorption (ΔH_i) for methanol and ethanol, as shown in Figure 7, decreased with

(27) Dubinin, M. M. *Characterization of Porous Solids*; Sing, K. S. W., Ed.; Society of Chemical Industries: London, 1979; Vol. 1, pp 1−11.

(28) Marsh, H. *Carbon* **1987**, *25*, 49.

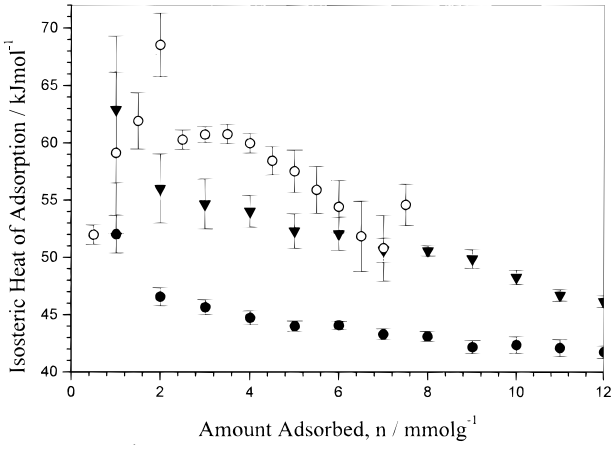

Figure 7. The variation of isosteric enthalpies of adsorption for methanol (●), ethanol (▼), and butan-1-ol (○) adsorption with amount adsorbed on active carbon BAX950.

increasing surface coverage. The values obtained for methanol adsorption were in the range 39−52 kJ mol^{-1}, with a limiting isosteric enthalpy of ∼57 kJ mol^{-1} at zero surface coverage. This compares with the enthalpy of vaporization[29] of 35.2 kJ mol^{-1} and an approximate value for the heat of adsorption, measured at low surface coverage by gas chromatographic methods for adsorption on graphitized thermal carbon black, of ∼ 45 kJ mol^{-1}.[30] Ethanol adsorption gave values in the range 44−63 kJ mol^{-1}. The corresponding values for the heat of vaporization[29] and low surface coverage enthalpy of adsorption[30] are 38.6 and ∼ 65 kJ mol^{-1}, respectively. The isosteric heats for butan-1-ol adsorption were in the range 51−69 kJ mol^{-1}. Previous studies have shown that the enthalpy of adsorption at low surface coverage was ∼80 kJ mol^{-1} [31] and the enthalpy of vaporization[29] was 43.3 kJ mol^{-1}.

A detailed analysis of the isosteric enthalpies and entropies of adsorption of methanol and ethanol on active carbon BAX950 are shown in Figure 8a. In the case of methanol there is little change in ΔS_i with surface coverage while ΔH_i decreases with increasing surface coverage. The trend for ethanol adsorption shows that both ΔS_i and ΔH_i decrease with increasing surface coverage. The corresponding data for isosteric enthalpies (ΔH_i) and entropies (ΔS_i) of adsorption for butan-1-ol as a function of surface coverage are shown in Figure 8b. Similar graphs were observed for the adsorption of *n*-octane and *n*-nonane on BAX950 (see Figure 8b). It is apparent that ΔH_i and ΔS_i become more negative with increasing surface coverage until a minimum is reached. This minimum corresponds to the point on the isotherm where the peak in the activation energy occurs. This peak in activation energy has been ascribed to preferential alignment of the butan-1-ol, *n*-octane, and *n*-nonane molecules in the pores.[8] In contrast, the graphs of ΔS_i and ΔH_i for the adsorption of methanol and ethanol show quite different trends.

4.3. Adsorption Kinetics. There is only limited information available concerning the adsorption kinetics of gases and vapors on activated carbons due to the complexity of the ultrahigh vacuum experimental techniques required for high-quality measurements, especially at low pressures (<1 mbar). Adsorption on active carbon involves diffusion through a porous system, which may have either slit-shaped or spherical characteristics. In the

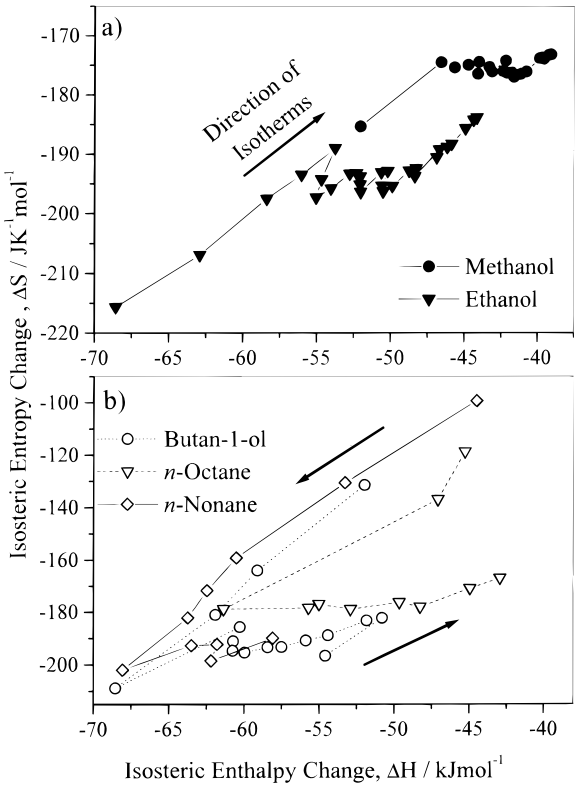

Figure 8. Variation of isosteric entropy with enthalpy of adsorption for (a) methanol (●, 288−313 K) and ethanol (▼, 293−313 K) and (b) butan-1-ol (○, 293−318 K), *n*-octane (▽, 288−313 K), and *n*-nonane (◇, 303−323 K) on active carbon BAX950.

Table 4. Molecular Sizes of the Adsorptives Used in This Study

adsorbate	MIN-1/Å	MIN-2/Å	MIN-3/Å
water[b]	2.917	3.226	3.888
methanol[a]	3.81	4.18	4.95
ethanol[a]	4.16	4.27	6.33
butan-1-ol[a]	4.16	4.46	8.91
n-octane[b]	4.014	4.524	12.833
n-nonane[b]	4.014	4.537	14.076

[a] Reference 33. Calculated by Dr. C. E.Webster and Dr. M. C. Zerner by the methods used in ref 32. [b] Reference 32.

case of the former, only one adsorptive dimension is critical, while for the latter, two dimensions are critical. The adsorption of alcohols on activated carbon involves interactions between the adsorbate and both the graphene layers and surface functional groups. The four alcohols were chosen because they have a combination of hydrophobic and hydrophilic character with a systematic change in chain length while the two other dimensions are kept essentially constant and together with water, *n*-octane, and *n*-nonane vapors studied previously form a suite of adsorptives covering a full range of hydrophilic/hydrophobic character. This minimizes differences in adsorption kinetics due to size dependent effects such as molecular sieving. The molecular dimensions obtained from ZINDO calculations for the suite of adsorptives are given in Table 4. The data indicate that the two smallest dimensions change by ∼0.35 and ∼0.36 Å for the series suite (excluding water).[32,33] The two minimum dimensions of water are

(29) CRC *Handbook of Chemistry and Physics*, 74th ed.; CRC Press: Boca Ratan, FL 1993.
(30) Kowalczyk, H.; Rychlicki, G.; Terzyk, A. P. *Pol. J. Chem.* **1993**, *67*, 2019.
(31) Avgul, N. N.; Kiselev, A. V. In *Chemistry and Physics of Carbon*; Walker, P. L., Jr., Ed.; Marcel Dekker: New York, 1970; Vol. 6, p 1.
(32) Webster, C. E.; Drago, R. S.; Zerner, M. C. *J. Am. Chem. Soc.* **1998**, *120*, 5509.

Table 5. Arrhenius Parameters for the Adsorption of Methanol, Ethanol, and on Active Carbon BAX950

a. Methanol and Ethanol

	methanol adsorption		ethanol adsorption	
relative pressure p/p^o	ln (A)/ln(s^{-1})	activation energy/kJ mol^{-1}	ln (A)/ln(s^{-1})	activation energy/kJ mol^{-1}
0−0.00099	10.32 ± 5.74	39.33 ± 2.30	13.36 ± 0.55	48.78 ± 4.74
0.00099−0.00196	6.56 ± 1.16	28.47 ± 0.46	9.33 ± 2.11	35.09 ± 3.79
0.00196−0.00293	6.62 ± 2.25	28.29 ± 0.90	6.94 ± 0.97	30.80 ± 2.46
0.00293−0.00391	6.10 ± 2.93	26.86 ± 1.17	6.65 ± 0.60	29.91 ± 1.52
0.00391−0.00489	6.10 ± 2.49	26.73 ± 1.00	6.81 ± 0.75	30.27 ± 1.89
0.00489−0.00973	6.61 ± 2.26	27.69 ± 0.91	5.76 ± 0.46	27.64 ± 1.13
0.00973−0.01953	5.23 ± 2.03	24.13 ± 0.81	4.66 ± 0.77	25.44 ± 1.94
0.01953−0.02935	5.74 ± 2.59	26.19 ± 1.03	4.57 ± 0.45	25.56 ± 1.13
0.02935−0.03906	3.33 ± 3.47	20.81 ± 1.39	4.55 ± 0.94	25.75 ± 2.43
0.03906−0.04890	3.68 ± 2.92	22.14 ± 1.17	3.21 ± 0.50	22.65 ± 3.03
0.04890−0.05875	2.48 ± 2.28	19.66 ± 0.91	1.19 ± 0.48	17.77 ± 1.26
0.05875−0.06861	2.36 ± 2.11	19.82 ± 0.85	1.68 ± 1.05	19.10 ± 1.21
0.06861−0.07824	3.17 ± 2.04	22.14 ± 0.75	−0.55 ± 0.22	13.57 ± 2.66
0.07824−0.08809	2.52 ± 2.40	20.80 ± 0.96	0.46 ± 0.22	16.18 ± 0.55
0.08809−0.09790	1.16 ± 0.88	17.63 ± 0.35	0.50 ± 0.63	16.34 ± 1.29
0.09790−0.10763	0.55 ± 1.16	16.35 ± 0.46	0.48 ± 0.92	16.49 ± 0.18
0.10763−0.11760	−0.50 ± 1.11	13.86 ± 0.44	−0.70 ± 0.75	13.47 ± 1.80
0.11760−0.12716	−0.23 ± 0.53	13.73 ± 1.26	0.78 ± 0.56	17.34 ± 1.41
0.12716−0.13694	0.12 ± 2.07	15.73 ± 0.83	−0.55 ± 0.50	13.94 ± 1.26
0.13694−0.14663	−0.52 ± 1.82	14.33 ± 0.73	−0.03 ± 0.15	15.22 ± 0.37
0.14663−0.15651	0.3 ± 1.22	16.45 ± 0.49	−0.45 ± 0.82	14.24 ± 2.05
0.15651−0.16632	−1.12 ± 1.36	12.98 ± 0.54	−1.03 ± 0.38	12.57 ± 0.94
0.16632−0.17613	−1.42 ± 1.71	12.29 ± 0.69	−2.38 ± 0.20	9.32 ± 3.73
0.17613−0.19583	−1.89 ± 0.90	11.27 ± 0.36	−0.45 ± 0.24	14.40 ± 2.52
0.19583−0.24465	−1.85 ± 0.55	11.70 ± 0.22	−0.94 ± 0.51	13.18 ± 1.28
0.24465−0.29367	−2.60 ± 1.30	9.94 ± 0.51	−2.10 ± 0.80	10.07 ± 0.67
0.29367−0.34208	−2.58 ± 0.54	10.07 ± 0.22	−1.61 ± 0.38	11.29 ± 0.96
0.34208−0.39098	−2.30 ± 1.16	8.90 ± 1.04	−3.00 ± 0.46	7.81 ± 1.68
0.39098−0.43942	−2.62 ± 0.54	10.04 ± 0.22	−1.84 ± 0.07	10.68 ± 0.17
0.43942−0.48851	−3.06 ± 1.54	8.86 ± 0.62	−3.54 ± 1.07	6.65 ± 2.70
0.48851−0.73306	−2.70 ± 0.42	10.00 ± 0.17	−3.58 ± 0.66	6.60 ± 1.39
0.73306−0.97721	−3.18 ± 1.22	10.27 ± 0.49	−3.66 ± 0.12	6.49 ± 0.31

b. Butan-1-ol

relative pressure p/p^o	ln (A)/ln(s^{-1})	activation energy/kJ mol^{-1}
0−0.00017	7.46 ± 1.33	37.46 ± 3.40
0.00017−0.0032	7.61 ± 1.67	36.60 ± 4.28
0.00032−0.00049	7.45 ± 1.23	35.80 ± 3.16
0.00049−0.00065	7.38 ± 0.23	35.31 ± 0.60
0.00065−0.00099	6.87 ± 0.44	33.90 ± 1.12
0.00099−0.00193	5.84 ± 0.43	31.65 ± 1.09
0.00193−0.00292	4.25 ± 0.22	26.76 ± 0.56
0.00292−0.00386	3.29 ± 0.27	24.10 ± 0.69
0.00386−0.00485	2.84 ± 0.28	22.80 ± 0.70
0.00485−0.00972	2.97 ± 0.06	23.03 ± 0.16
0.00972−0.01945	2.19 ± 0.12	20.97 ± 0.31
0.01945−0.02918	2.69 ± 0.14	22.12 ± 0.35
0.02918−0.03892	2.21 ± 0.37	20.87 ± 0.94
0.03892−0.04865	4.54 ± 0.51	26.63 ± 1.29
0.04865−0.05834	5.09 ± 0.41	27.88 ± 1.03
0.05834−0.06808	6.02 ± 0.13	30.10 ± 0.33
0.06808−0.07781	5.62 ± 0.08	29.07 ± 0.21
0.07781−0.08755	4.96 ± 0.12	29.86 ± 0.32
0.08755−0.09728	3.75 ± 0.49	24.21 ± 1.24
0.09728−0.10701	3.74 ± 0.40	24.16 ± 1.00
0.10701−0.11653	3.7 ± 0.39	23.96 ± 0.99

∼0.9−1.0 Å smaller than the minimum dimensions of methanol.

The adsorption kinetics for all four alcohols on BAX950 followed a linear driving force model over the p/p^o range 0−0.97. The rate constant increases to a maximum at p/p^o ∼ 0.02 for methanol and ethanol and then decreases steadily with relative pressure and surface coverage. The maximum in the rate constants for methanol and ethanol adsorption occur at relative pressures that correspond to the deviations from linearity observed in the D−R plots (See Figure 6). It is reasonable to conclude that barriers develop during the adsorption process that cause a decrease in rate constant, associated with curvature in the D−R plot. The observation of pore-width-dependent ordering of ethanol molecules confined in graphite slit nanospaces[16] may be related to the development of barriers to diffusion. For propan-1-ol and butan-1-ol the rate increases to a maximum at a relative pressure of ∼0.06, corresponding to complete filling of the micropore volume, after which a plateau is reached.

4.4. Adsorption Activation Energies. The barriers to diffusion for the adsorption of methanol, ethanol, and butan-1-ol vapors on BAX950 over the range $p/p^o \sim 0-0.97$ were calculated for the various relative pressure incre-

(33) Webster, C. E.; Zerner, M. C. Personal communication.

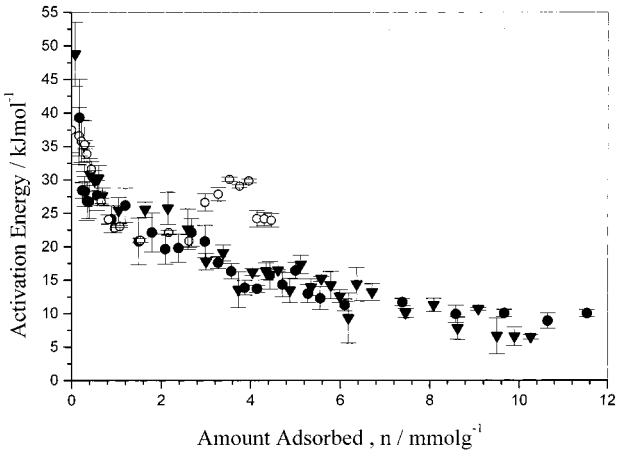

Figure 9. Variation of activation energies for adsorption of methanol (●), ethanol (▼), and butan-1-ol (○) vapor with relative pressure on active carbon BAX950 with amount adsorbed; temperature range, 288−318 K.

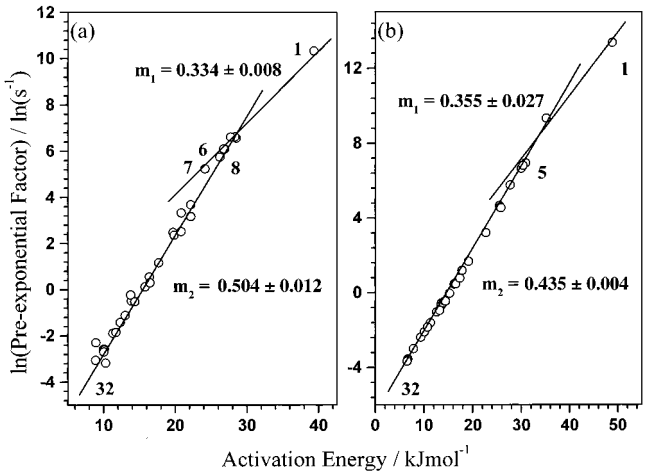

Figure 10. Variation of ln(preexponential factor) (ln (*A*)) with activation energy (E_a) for adsorption of a) methanol and b) ethanol on active carbon BAX950 showing the numbering of the pressure steps.

ments using the Arrhenius equation. The pressure increases were carried out in relative pressure terms and the activation energies correspond to changes in specific surface coverage. Table 5 shows the activation energies and corresponding ln(preexponential factors) (ln (*A*)) for adsorption over the relative pressure range $p/p^o = 0-0.97$. Figure 9 shows the activation energies for methanol, ethanol, and butan-1-ol adsorption on BAX950 as a function of the amount adsorbed. The activation energies cover the range up to ~40 kJ mol^{-1}, and similar values have been obtained previously for separate investigations with *n*-octane,[8] *n*-nonane,[8] and water[5] adsorption on active carbon BAX950 and for the diffusion of oxygen, nitrogen, argon, etc. on carbon molecular sieves.[3,4,34] It is apparent from Figure 9 that the highest activation energy value was obtained for the lowest surface coverage, where molecular sieving effects occur in the microporosity. The graph of activation energy versus relative pressure for butan-1-ol adsorption shows a peak at $p/p^o \sim 0.1$ (liquid volume adsorbed = 0.40 cm^3 g^{-1}), similar to peaks observed for *n*-octane (0.48 cm^3 g^{-1}) and *n*-nonane (0.34 cm^3 g^{-1}) adsorption.[8] It is likely that alignment of the longer chain molecules in the pores leads the cooperative effects and the development of barriers to diffusion.[8]

4.5. Compensation Effect. The compensation effect in adsorption kinetics involves the linear relation

$$\ln(A) = mE_a + c \qquad (5)$$

where *A* is the preexponential factor, E_a is the activation energy, and *m* and *c* are the gradient and intercept of the compensation graph. This leads to the equation

$$\ln(k) = E_a\left(m - \frac{1}{RT}\right) + c \qquad (6)$$

where E_a is in units of J mol^{-1}. If $m > 1/RT$, then ln(*k*) will increase with increasing activation energy (E_a), whereas if $m < 1/RT$, then ln(*k*) will decrease with increasing activation energy.

The compensation effect has been reported for a wide range of heterogeneous catalytic[35−40] and homogeneous chemical reactions.[41] The effect has also been reported for thermally activated processes such as electronic conductivity in semiconductor systems[42,43] and thermal desorption.[44−48] The observation of the compensation effect for widely different processes has led to a number of explanations. Some researchers[5] have proposed that the compensation effect is, in some cases, a result of statistical and experimental errors,[49] while other workers have argued that in the case of reaction kinetics it is a direct consequence of the Arrhenius and Eyring equations.[39,40] Several studies have attempted to show that the effect arises from dynamic processes.[44−48,50−52] However, while it is well-known as a phenomenological effect, its interpretation remains controversial. As a result, the compensation effect has often been reported as an observation with no conclusions drawn with regard to its real meaning. Agrawal[53,54] suggested that for a "true" compensation effect a plot of ln (*A*) against E_a will have a linear dependency with all the Arrhenius plots in a series meeting at a concurrent point, known as the isokinetic point with ln(k_{iso}) being nonzero. The compensation effects observed for the adsorption of the suite of adsorptives studied have characteristic isokinetic temperatures and nonzero rate constants at this temeprature.

Figure 10 shows good linear correlation between ln (*A*) and the activation energy, indicative of a compensation effect for the adsorption of both methanol and ethanol on BAX950. The values of *m*, the gradient of the compensation graphs, for methanol and ethanol were 0.551 ± 0.009 and 0.443 ± 0.003 ln(s^{-1}) mJ^{-1} mol, respectively. The direction of increasing surface coverage is indicated on the graph

(34) Chagger, H. K.; Ndaji, F. E.; Sykes, M. L.; Thomas, K. M. *Carbon* **1995**, *33*, 1405.
(35) Galwey, A. K. *J. Catal.* **1983**, *84*, 270.
(36) Galwey, A. K. *Adv. Catal.* **1977**, *26*, 247.
(37) Conner, W. C., Jr. *J. Catal.* **1983**, *84*, 273.
(38) Patterson, W. R.; Rooney, J. J. *J. Catal.* **1994**, *146*, 310.
(39) Schwab, G. M. *J. Catal.* **1983**, *84*, 1.
(40) Rooney, J. J. *Appl. Catal.* **1995**, *123*, 10.
(41) Leffler, J. E. *J. Org. Chem.* **1955**, *20*, 1202.
(42) Meyer, W.; Nedel, H. *Z. Tech. Phys.* **1937**, *12*, 588.
(43) Dyre, J. C. *J. Phys. C* **1986**, *19*, 5655.
(44) Payne, S. H.; Kreuzer, H. J. *Surf. Sci.* **1989**, *222*, 404.
(45) Sommer, E.; Kreuzer, H. J. *Phys. Rev. Lett.* **1982**, *49*, 61.
(46) Sommer, E.; Kreuzer, H. J. *Phys. Rev. B* **1982**, *26*, 4094.
(47) Kreuzer, H. J.; March, N. H. *Theor. Chim. Acta* **1988**, *74*, 339.
(48) Kreuzer, H, *J. Chem. Soc., Farad. Trans.* **1990**, *86*, 1299.
(49) Suarez, M. P.; Palermo, A.; Aldao, C.M. *J. Thermal. Anal.* **1994**, *41*, 807.
(50) Peacock-Lopez, E.; Suhl, H. *Phys. Rev. B* **1982**, *26*, 3774.
(51) Zhdanov, V. P. *Surf. Sci.* **1985**, *159*, L416.
(52) Zhdanov, V. P. *J. Phys. Chem.* **1989**, *93*, 5582.
(53) Agrawal, R. K. *J. Thermal Anal.* **1986**, *31*, 73.
(54) Agrawal, R. K. *J. Thermal Anal.* **1989**, *35*, 909.

Table 6. Gradients and Intercepts of Compensation Graphs and Isokinetic Rates and Temperatures for the Adsorption of Methanol, Ethanol, Butan-1-ol, *n*-Octane, *n*-Nonane and Water Vapors on Activated Carbon BAX950

adsorbate	pressure steps	compensation gradient/-$\ln(s^{-1})$ $mmol^{-1}$ J	ln (*A*) at zero activation energy/-$\ln(s^{-1})$	isokinetic temp/K	isokinetic rate/$s^{-1} \times 10^{-4}$
methanol	1−6	0.334 ± 0.008	−2.83 ± 0.25	360.1 ± 8.6	590.1 ± 52.1
	6−32	0.504 ± 0.012	−7.57 ± 0.21	238.6 ± 5.7	5.2 ± 0.1
ethanol[a]	1−5	0.355 ± 0.027	−3.83 ± 0.97		
	5−32	0.435 ± 0.004	−6.55 ± 0.06	276.5 ± 2.5	14.3 ± 0.1
butan-1-ol	1−13	0.354 ± 0.004	−5.15 ± 0.11	339.8 ± 3.8	58.0 ± 1.2
	13−16	0.412 ± 0.004	−6.40 ± 0.10	291.9 ± 2.8	16.6 ± 0.3
	16−21	0.381 ± 0.003	−5.47 ± 0.09	315.7 ± 2.5	42.1 ± 0.7
n-octane	1−9	0.307 ± 0.012	−2.91 ± 0.33	391.8 ± 15.3	544.8 ± 61.8
	9−13	0.450 ± 0.009	−5.78 ± 0.23	267.3 ± 5.3	30.9 ± 1.2
	13−22	0.345 ± 0.014	−2.58 ± 0.32	348.6 ± 14.1	757.7 ± 94.0
n-nonane	1−5	0.250 ± 0.050	−2.75 ± 1.25	481.1 ± 96.2	639.3 ± 290.6
	5−9	0.427 ± 0.008	−6.83 ± 0.20	281.7 ± 5.3	10.8 ± 0.3
	9−27	0.345 ± 0.003	−4.28 ± 0.07	348.6 ± 3.0	138.4 ± 2.3
water	1−4	0.335 ± 0.006	−4.68 ± 0.18	359.0 ± 6.4	92.8 ± 3.6
	4−8	0.459 ± 0.012	−10.14 ± 0.37	262.0 ± 6.9	0.39 ± 0.01

[a] Isokinetic parameters were not calculated for steps 1−5 because of the limited accuracy of the compensation gradient for the initial adsorption.

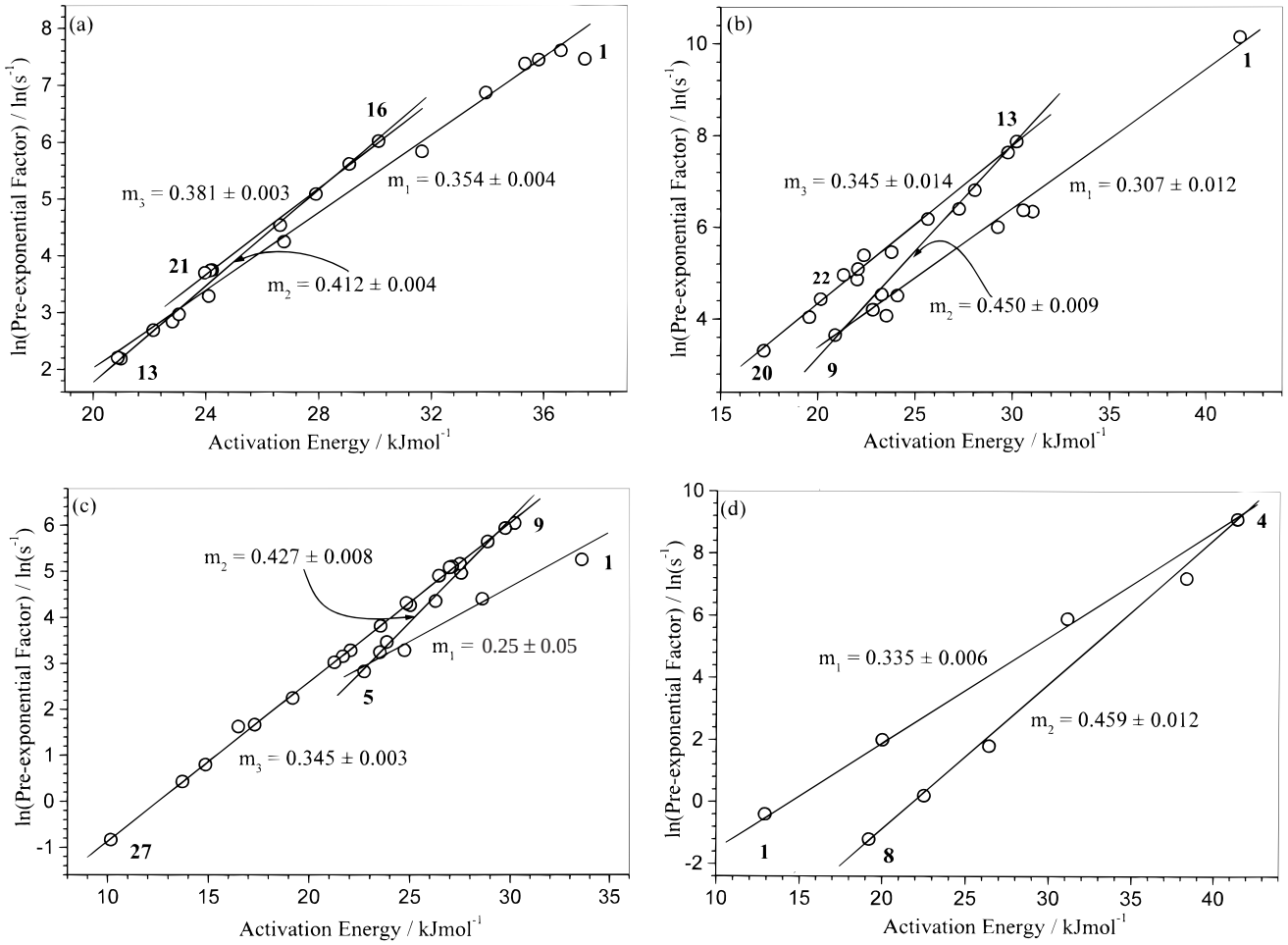

Figure 11. Variation of ln(preexponential factor) (ln (*A*)) with activation energy (E_a) for adsorption of (a) butan-1-ol, (b) *n*-octane, (c) *n*-nonane, and (d) water vapors on active carbon BAX950 showing the numbering of the pressure steps.

by the numbering of some isotherm points. However, Figures 4 and 5 show that both ethanol and methanol adsorption have peaks in the ln(*k*) versus surface coverage (*n*) graphs at isotherm points ∼6−7 and 5, respectively. Therefore, the gradients of compensation graphs were examined before and after the peaks for both adsorptives and the results are shown in Table 6 and Figure 10. The accuracy of the results for the estimation of the compensation gradient is limited by the relatively small number of measurements available. However, in the case of methanol vapor adsorption, the compensation gradient changes at the peak in ln(*k*) from 0.334 ± 0.008 $\ln(s^{-1})$ mJ^{-1} mol ($m < 1/RT$) before the peak to 0.504 ± 0.012 $\ln(s^{-1})$ mJ^{-1} mol ($m > 1/RT$) after the peak ($1/RT = 0.397$ mol mJ^{-1} at 303 K). It is apparent that the compensation gradients (*m*) before and after the peak in rate constant are significantly different. In the case of ethanol adsorption, the differences in the compensation gradients are close to the experimental uncertainties in the values due to the limited availability of data in the initial region of

the graph. The compensation gradients were 0.355 ± 0.027 $\ln(s^{-1})$ mJ^{-1} mol for the initial region before the peak in the rate constant with surface coverage and 0.435 ± 0.004 $\ln(s^{-1})$ mJ^{-1} mol after the peak. It is apparent that the results for the compensation graphs for methanol and ethanol adsorption are consistent

Figure 11a shows the corresponding graph of ln (A) versus E_a for butan-1-ol adsorption. It is evident that there is a compensation graph with gradient 0.337 ± 0.011 $\ln(s^{-1})$ mJ^{-1} mol, but closer inspection shows a more complex graph corresponding to changes associated with the development of a peak at $p/p^o = 0.1$ (adsorbed liquid volume 0.4 cm^3 g^{-1}), where the gradient changes from 0.354 ± 0.004 (pressure steps 1−13) to 0.412 ± 0.004 (pressure steps 13−16) to 0.381 ± 0.003 $\ln(s^{-1})$ mJ^{-1} mol (pressure steps 16−21) (see Table 6). The three regions of the compensation graph for adsorption of butan-1-ol on active carbon BAX950 correspond approximately to pressure steps 1−13, for the decrease in E_a to a minimum before the peak due to cooperative effects, steps 13−16 correspond to an increase from the minimum to the peak due to cooperative effects, and steps 16−21 correspond to the final part of the isotherm above the peak in the activation energy due to alignment of the long chain molecules leading to cooperative effects. Detailed analysis of the adsorption kinetic data for *n*-octane and *n*-nonane[8] also shows compensation graphs (see Figure 11b,c) with three regions, and the corresponding gradients of the three plots of the compensation graph are shown in Table 6.

The changes in the compensation gradients with adsorption mechanism have implications for the variation of ln(k) with activation energy which can be inferred from eq 6 and the relative values of the compensation gradient (m) and $1/RT$. Graphs of rate constant (k) versus E_a for methanol and ethanol adsorption on active carbon BAX950 are shown in parts a and b of Figure 12, respectively. It is evident that for the adsorption of methanol vapor the rate constant (k) increases with increasing E_a, which is the situation when $m > 1/RT$ for steps 6−32, but decreases with increasing E_a for steps 1−6, where $m < 1/RT$. In the case of the latter, there are only a limited number of data points available. The results for the adsorption of ethanol vapor show similar trends. The adsorption of butan-1-ol on active carbon BAX950 shows that there are changes in the trend from rate constant (k) decreasing with increasing E_a (steps 1−13) to rate constant (k) increasing with increasing E_a (steps 13−16) and back again (steps 17 and above)(see Figure 13a). The thermodynamic data show that the peak associated with the cooperative effect is accompanied by the largest negative value of ΔS_i, i.e., a system with the highest order. The kinetic data for adsorption of *n*-octane and *n*-nonane on BAX950 also show similar trends in relation to m and $1/RT$, and the trends in rate constant (k) in relation to E_a are those expected for the compensation gradients (see Figure 13b,c). The thermodynamic data for *n*-octane and *n*-nonane adsorption on BAX950 also show trends similar to butan-1-ol (see Figure 8b). Butan-1-ol, *n*-octane, and *n*-nonane adsorption on BAX950 all show evidence of a peak in the E_a versus relative pressure graphs due to cooperative effects in the adsorption process resulting from the ordering of longer chain molecules in the porosity.

A similar effect has been observed for water[5] adsorption on BAX950 with two components to the compensation graph corresponding to either side of the peak in the activation energy versus relative pressure graph. In this case the values of the gradients (m) of the compensation graphs were 0.335 ± 0.006 and 0.459 ± 0.012 $\ln(s^{-1})$ mJ^{-1} mol for p/p^o steps $\leq 0.427-0.512$ and $\geq 0.427-0.512$,

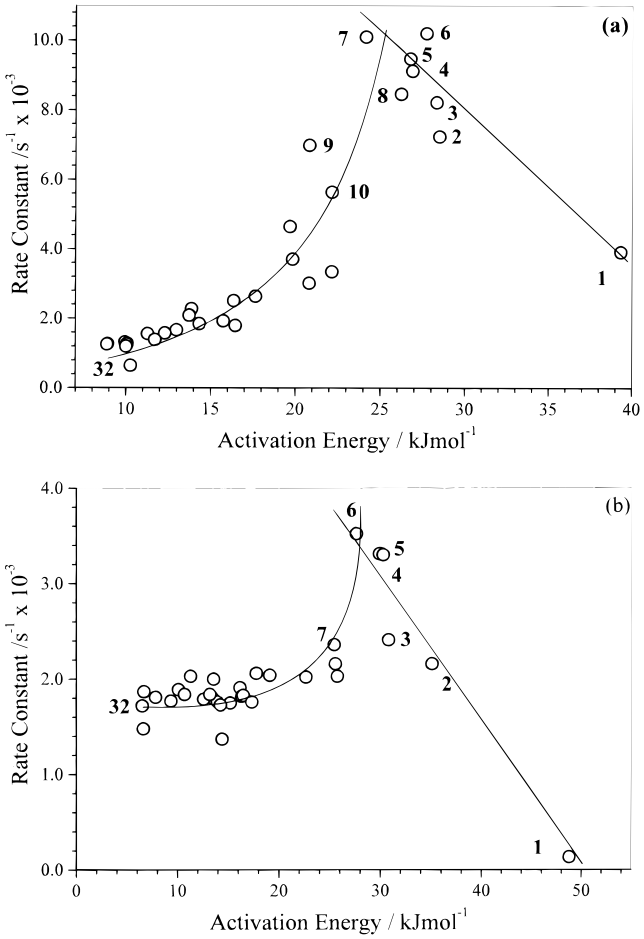

Figure 12. The variation of rate constant (k) at 303 K with E_a for the adsorption of (a) methanol and (b) ethanol on active carbon BAX950 showing the numbering of the pressure steps.

respectively, as shown in Figure 11d. This corresponds to rate constant (k) decreasing with increasing E_a for p/p^o steps $\leq 0.427-0.512$ and rate constant (k) decreasing with decreasing E_a for p/p^o steps $\geq 0.427-0.512$ (see Figure 13d). In the case of adsorption of water vapor on carbon C1, the amount adsorbed was much lower ($^1/_5$) than for BAX950, and the activation energies for adsorption were lower and in a narrower range, leading to higher uncertainties in the measurements.[5] The trends in the rate constant with E_a are apparent from the graphs of rate constant (k) versus p/p^o, where the rate constants decrease with increasing relative pressure for adsorption on BAX950 but go through a minimum for carbon C1 while the trends in activation energy are similar.[5] However, the uncertainties in the compensation gradients and limited availability of data do not allow detailed comparisons.

It is apparent that the graphs of ln (A) versus E_a, which demonstrate the compensation effect while showing the same general trend, also exhibit regions with different gradients which are a consequence of the adsorption mechanism and the development of barriers to diffusion during the adsorption process. The observation of different gradients for the compensation effect related to the mechanisms was confirmed by the identification of clearly different isokinetic temperatures and nonzero isokinetic rate constants for each region of the graph. Typical examples of the graphs showing the isokinetic temperatures and rate constants are given in Figures 14 a−d. It is interesting to note that for each adsorbate/adsorbent system there are examples of the isokinetic temperature being both above and below the temperature range for

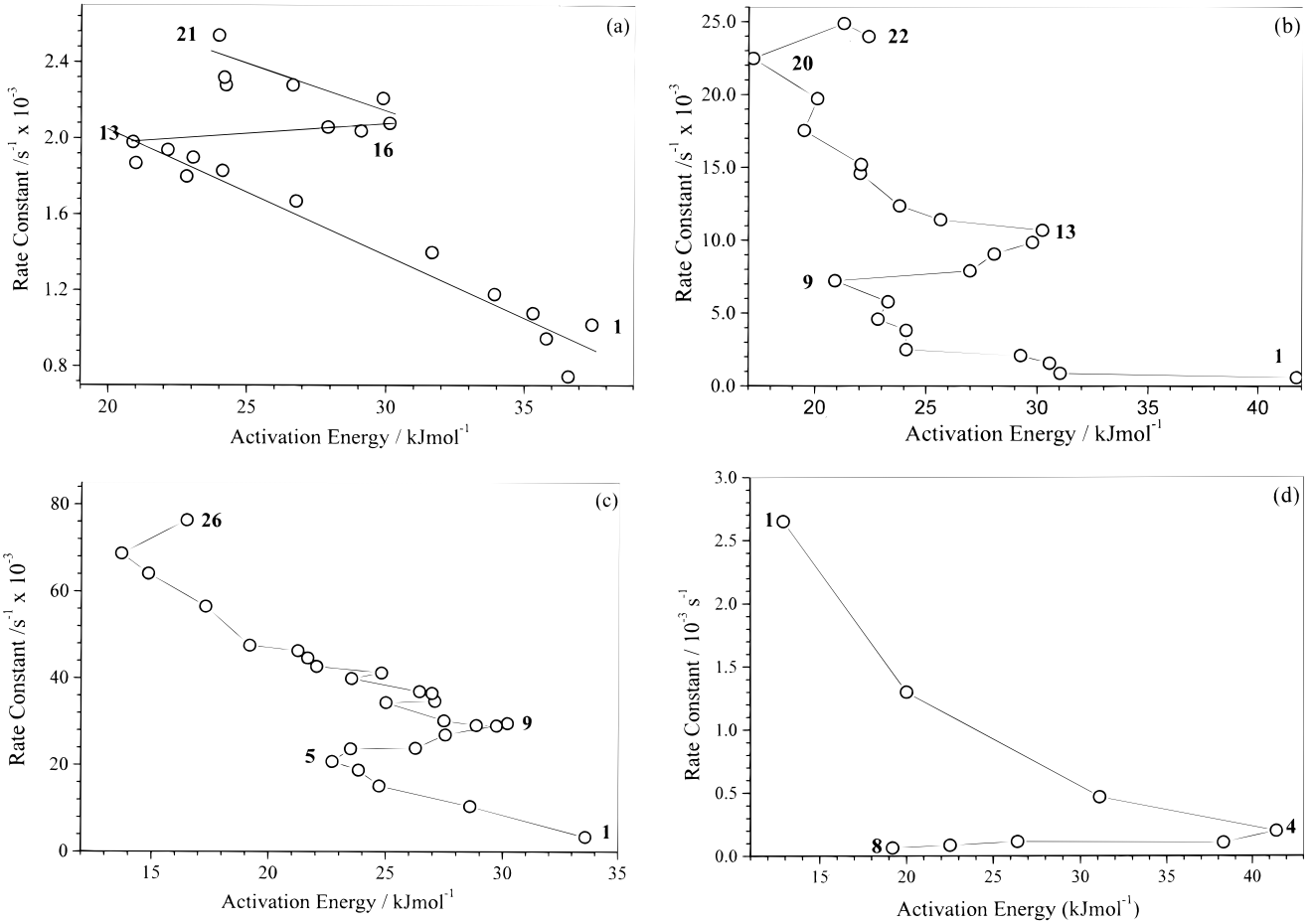

Figure 13. The variation of rate constant (k) at 303 K with E_a for the adsorption of (a) butan-1-ol, (b) *n*-octane, (c) *n*-nonane, and (d) water vapors on active carbon BAX950 showing the numbering of the pressure steps.

the kinetic measurements, depending on the amount adsorbed and adsorption mechanism. Table 6 provides details of these parameters, which confirm the validity of the compensation effect in each case. In the case of water vapor adsorption this involves the development of clusters of water molecules around functional groups in the active carbon; for methanol and ethanol, pore-width-dependent ordering processes may be involved,[16] while in the case of butan-1-ol, *n*-octane, and *n*-nonane, the relatively long chain molecules orient themselves in the pores leading to cooperative effects. Clearly the value of the compensation gradient reflects the adsorption mechanism in the particular pore structure, leading to the development of diffusion barriers.

It is noteworthy that the values of the gradients of the compensation graphs are similar, even though the six adsorbent−adsorbate systems studied cover a varied range of isotherm type. This establishes that the compensation effect occurs for a wide range of adsorptives ranging from hydrophilic to hydrophobic in character for a single active carbon adsorbent (BAX950) where the LDF model is obeyed. The compensation graphs for the adsorption of the suite of adsorptives on BAX950 cover isotherm types I−III and these are compared in Figure 15. It is apparent that the graphs are very similar.

Previous studies of water vapor adsorption on a highly microporous carbon (C1) also showed that the isotherm was type V and that the kinetic data obeyed the LDF model and exhibited a compensation effect. The activation energies and preexponential factors for a range of adsorptives on a carbon molecular sieve where the LDF model is followed[3,4] also fit on the overall compensation graph shown in Figure 15. Furthermore, recent studies of the adsorption of methanol on a porous framework material, $Ni_2(4,4'\text{-bipy})_3(NO_3)_4$, which has a uniform porosity of 7 × 11 Å, also shows that the kinetic data follow an LDF model and exhibit a compensation effect. These data for adsorption of various adsorptives on a range of adsorbents show that when the adsorption kinetics follow the LDF model, a compensation effect is observed.[55] The results suggest that the compensation effect may be widely applicable to the adsorption kinetics for diffusion into porous solids.

Previous studies have also shown that the adsorption kinetics may follow an LDF, combined barrier resistance/diffusion, or Fickian diffusion model, depending on the nature of the adsorptives and adsorbent as well as the experimental conditions. Reid et al.[3,4] showed that that the kinetic model for adsorption of carbon dioxide on a CMS changed from LDF, through combined barrier resistance/diffusion, to Fickian diffusion kinetic models with changes in pressure and temperature. The LDF model is based on a uniform concentration on each side of the barrier, whereas, for Fickian diffusion, the diffusion is related to the concentration gradient. The combined barrier-resistance/diffusion model is a combination of these two extremes. It is reasonable to expect the concentration gradient to influence the diffusion through the barrier. The data for the barrier resistance constant (k_b) and the diffusion constant (k_d) obtained previously[3,4] from the combined barrier resistance/diffusion model[56] for carbon dioxide adsorption on a CMS were fitted to

(55) Fletcher, A. J.; Thomas, K. M. Unpublished results.

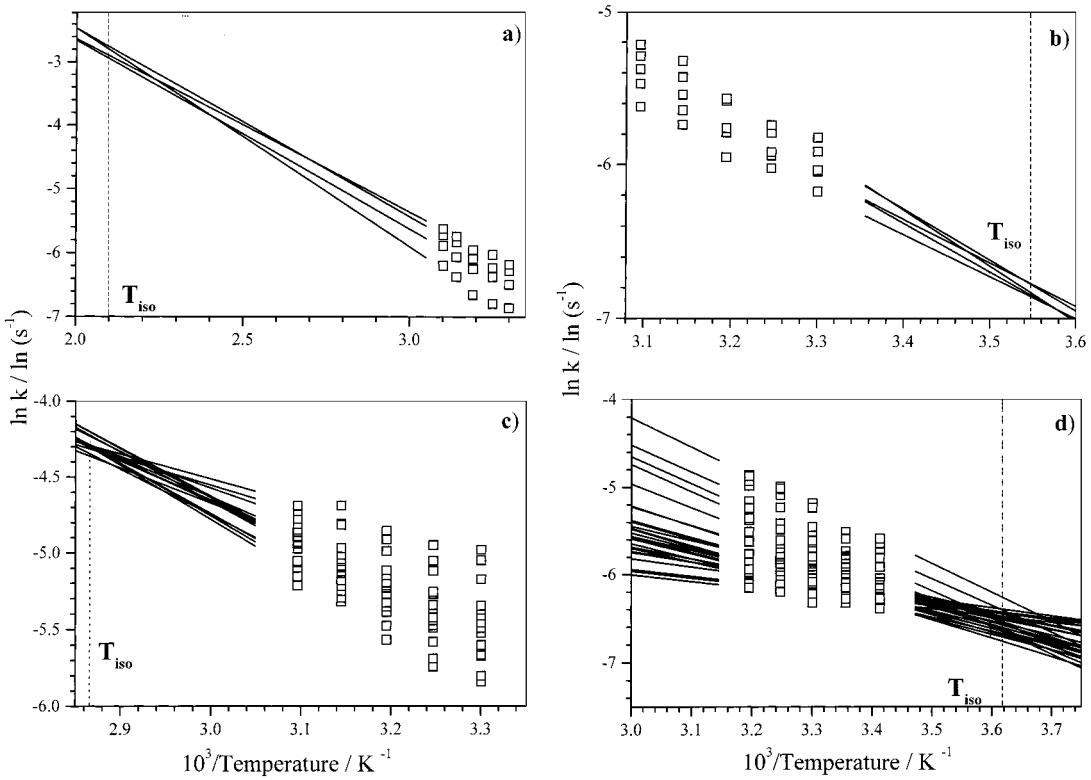

Figure 14. Arrhenius graphs showing the isokinetic temperatures and rate constants for (a) *n*-nonane (steps 1−5), (b) *n*-nonane (steps 5−9), (c) *n*-nonane (steps 9−27), and (d) ethanol (steps 5−32),

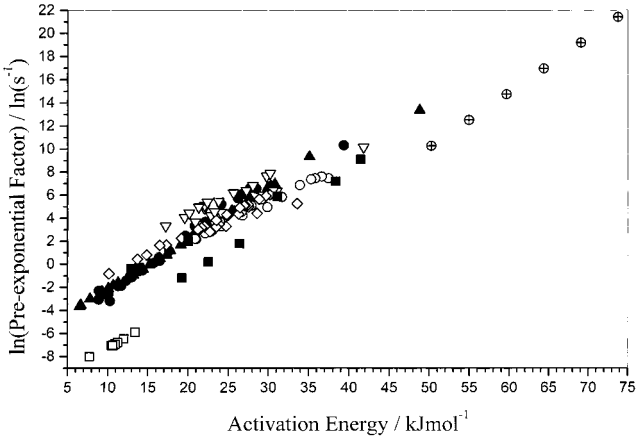

Figure 15. Variation of ln-(preexponential factor (ln(A))) with activation energy E_a for adsorption of vapors (a) methanol (●), ethanol (▼), butan-1-ol (○), water (■), *n*-octane (▽) and *n*-nonane (◇) on BAX950 and (b) carbon dioxide on CMS for diffusion constant k_d (□) and barrier resistance constant k_b (⊕).

linear relations between ln(k) and the surface coverage (n) for a given temperature, and these relations were used to determine the Arrhenius parameters at constant surface coverage. Typical values of ln (A) and E_a for k_d were in the range −6 to −8 ln(s^{-1}) and 8−14 kJ mol^{-1}, respectively. The values of ln (A) and E_a at zero surface coverage for k_b were 10.4 ± 0.6 ln(s^{-1}) and 50.6 ± 1.6 kJ mol^{-1}, respectively, and both of these values increased with increasing surface coverage. It is apparent that a compensation effect exists for both k_b and k_d that follows a similar trend to the other adsorbate/adsorbent systems but with k_b having higher ln (A) and E_a values and k_d having lower ln (A) and E_a values. These results suggest that the general relation between ln (A) and E_a for adsorption kinetics may extend further. The corresponding graphs of the Arrhenius parameters calculated from the diffusion and barrier component parts of the model for adsorption of carbon dioxide on a carbon molecular sieve are compared with adsorption results for the suite of adsorptives on BAX950 in Figure 15. It is evident that the compensation graphs follow similar trends.

The explanation of the compensation effect for adsorption/desorption kinetics in porous solids is consistent with a model that includes two factors in the adsorption kinetics: (a) diffusion along the pores and (b) diffusion through the barrier at the pore entrance.[57,58] The adsorption kinetics follow the LDF model, which is consistent with diffusion through a barrier being the rate-determining step rather than diffusion along the pores. In all cases, ln (A) increases with increasing activation energy. This can be ascribed to the activation energy for diffusion through the barrier influencing the number of molecules in front of the barrier, thereby causing a change in the preexponential factor. A high activation energy results in an increase in the number of molecules in front of the barrier, leading to a corresponding increase in the preexponential factor and vice versa. Hence, the activation energy and ln(preexponential factor) parameters are related. The results suggest that the mechanism by which the diffusion barrier is developed influences the compensation gradient and that the compensation effect may be applicable to adsorption on a wide range of microporous materials.

4.6. Desorption Kinetics. There is very limited literature concerning the desorption kinetics of gases and vapors on activated carbons, again due to the complexity

(56) Loughlin, K. F.; Hassan, M. M.; Fatehi, A. I.; Zahur, M. *Gas Sep. Purif.* **1993**, *7*, 264.

(57) Rao, M. B.; Jenkins, R. G.; Steele, W. A. *Extended Abstracts, Biennial Conference on Carbon*; American Carbon Society: Lexington, Kentucky, 1985; Vol. 17, p 114.

(58) Rao, M. B.; Jenkins, R. G.; Steele, W. A. *Langmuir* **1985**, *1*, 137.

of the experimental techniques involved. The desorption kinetics of methanol vapor from BAX950 follows an LDF model. Previous studies have shown that both *n*-octane vapor desorption from BAX950[8] and water vapor desorption from a highly microporous carbon[5] also follow an LDF model. A peak is observed at $p/p^o = 0.02$ as in the case of adsorption, after which the rate decreases with decreasing relative pressure. The values obtained for the desorption rate constants are similar to those for the adsorption process, with only a slight variation at very low pressure, where the desorption rates are slower than adsorption. This observation may be ascribed to difficulty for the desorption of methanol from ultramicroporosity; similar observations have been made with water desorption from BAX950.[5] In the case of *n*-octane desorption, the rate constants were always significantly slower than the adsorption rate constants for the corresponding pressure step.[8]

The information available on the compensation effect for desorption kinetics is more limited. However, calculations of thermal desorption from graphite surfaces have suggested that a compensation effect exists.[44−48] Previous studies have shown that desorption of water vapor from a highly microporous carbon derived from coconut shell (type V isotherm) and *n*-octane desorption from a wood-derived active carbon (BAX950) (type I isotherm) both follow the LDF model and exhibit a compensation effect. The activation energies for desorption are usually in the range ~5−20 kJ mol^{-1}, and the precision of these values is limited by the relatively small change in rate constant with temperature. There is no unequivocal evidence for different compensation gradients within the overall compensation graphs as is the case for adsorption.

The desorption kinetics follow an LDF model and this is consistent with diffusion through barriers in the porosity being the rate-determining step. In this case the adsorbate concentration inside the particle is higher than the equilibrium value and the adsorbate has to diffuse through the barriers in the porosity to equilibrate with the gas/vapor phase. A high activation barrier results in a build-up before the barrier, leading to an increase in ln (*A*) and vice versa. Therefore, the activation energy and preexponential factor are not independent parameters and a compensation effect is observed. Since the desorption studies cover different carbon adsorbents and both hydrophilic and hydrophobic adsorptives, the results suggest that the compensation effect may also be widely applicable to desorption kinetics which obey the LDF model.

5. Conclusions

The adsorption of methanol, ethanol, propan-1-ol, and butan-1-ol vapor on active carbon BAX950 has been investigated and, in combination with previous studies on water, *n*-octane, and *n*-nonane adsorption, provides data for a suite of adsorptives with varying hydrophilic/hydrophobic character. The barriers to diffusion into the adsorbent were produced by a number of mechanisms, including molecular sieving, clustering of water molecules around functional groups, pore-width-dependent ordering in the case of ethanol, and cooperative effects for the adsorptives with the longest chain lengths (butan-1-ol, *n*-octane, and *n*-nonane).

The compensation effect is observed for adsorbate−adsorbent systems with varying isotherm shape from type I to type III and type V and rate constants which have a wide range of trends varying from rate constants increasing with increasing surface coverage to rate constants decreasing with increasing surface coverage. The compensation effect graphs have regions with different compensation gradients, isokinetic temperatures, and isokinetic rate constants that result from changes in the adsorption mechanism. The compensation gradients can be used to explain the change in rate constant in relation to the barriers to diffusion developed during the adsorption process. The change in compensation gradient for water vapor adsorption is associated with the pore-filling region where bridging between clusters of water molecules occurs. Initially the rate decreases with increasing E_a until the pore-filling region is reached and then decreases with decreasing E_a for BAX950, while the situation for a highly microporous carbon is similar in the initial region but has ln(k) increasing with decreasing E_a above the peak in the activation energy. The variation in the compensation effects for methanol and ethanol adsorption on BAX950 are very similar and consistent with a peak in ln(k) at low relative pressure. Variation in the compensation effect with a mechanism for butan-1-ol, *n*-octane, and *n*-nonane adsorption gave different gradients for the compensation graphs associated with a decrease in E_a to the minimum prior to the peak due to cooperative effects, an increase to the peak due to cooperative effects, and a decrease in E_a above this peak.

In the adsorption systems studied the LDF model is obeyed and diffusion through a barrier at the pore entrance is the rate-determining step. A high barrier to diffusion leads to build-up of adsorbate in front of the barrier, which gives a high preexponential factor and vice versa. This gives rise to a compensation effect between ln (*A*) and E_a. The compensation effect was also observed for the desorption kinetics for hydrophobic and hydrophilic adsorptives on active carbons which gave type I and III isotherms, respectively. The results suggest that the compensation effect for adsorption/desorption kinetics is quite general for adsorption on active carbons, and there is some evidence that it may extend to microporous solids in general.

Acknowledgment. The research was supported by the EPSRC under a grant and studentship for A.J.F. The authors would like to thank Dr. C. E. Webster, Texas A & M University, and the late Dr. M. C. Zerner of University of Florida for the calculations of the molecular dimensions of the adsorptives.

LA9916528